Confined Water: A Mercedes-Benz Model Study

T. Urbic,[†] V. Vlachy,[†] and K. A. Dill*[,‡]

Faculty of Chemistry and Chemical Technology, University of Ljubljana, Aškerčeva 5, SI-1000 Ljubljana, Slovenia, and Department of Pharmaceutical Chemistry, University of California, San Francisco, California 94143-1204

Received: September 29, 2005; In Final Form: January 16, 2006

We study water that is confined within small geometric spaces. We use the Mercedes-Benz (MB) model of water, in NVT and μVT Monte Carlo computer simulations. For MB water molecules between two planes separated by a distance d, we explore the structures, hydrogen bond networks, and thermodynamics as a function of d, temperature T, and water chemical potential μ. We find that squeezing the planes close enough together leads to a vaporization of waters out of the cavity. This vaporization transition has a corresponding peak in the heat capacity of the water. We also find that, in small pores, hydrogen bonding is not isotropic but, rather, it preferentially forms chains along the axis of the cavity. This may be relevant for fast proton transport in pores. Our simulations show oscillations in the forces between the inert plates, due to water structure, even for plate separations of 5−10 water diameters, consistent with experiments by Israelachvili et al. [*Nature* **1983**, *306*, 249]. Finally, we find that confinement affects water's heat capacity, consistent with recent experiments of Tombari et al. on Vycor nanopores [*J. Chem. Phys.* **2005**, *122*, 104712].

1. Introduction

We study here water that is sterically confined to small spaces. Such situations arise when water is in pores, for example, in membrane protein channels,[1−3] such as aquaporins, in rocks and minerals, or between plates in force microscopy experiments. Such confinement can affect the structure of water, through the restriction it imposes on the hydrogen bonding network. Confined water can thus have different properties than bulk water. Surfaces often result in a local ordering of nearby waters, due to the imposition of geometric constraints on hydrogen bonding patterns.[4] Water in the vicinity of surfaces has been studied extensively;[5−22] a more complete review is given in ref 23.

A set of studies in three dimensions very similar to this work has been published by Choudhury et al.[24,25] The hydration behavior of two planar nanoscopic hydrophobic solutes in liquid water was studied by calculating the potential of mean force between them at constant pressure as a function of the solute-solvent interaction potential.

For this study of confinement, we use the Mercedes-Benz model of water.[26−31] This is a two-dimensional simplified model. Each water molecule is modeled as a disk that interacts with other such waters through the following: (1) a Lennard-Jones (LJ) interaction and (2) an orientation-dependent hydrogen bonding interaction through three radial arms arranged as in the Mercedes-Benz (MB) logo. The hydrogen bonding interaction is a Gaussian function of angle and distance. Bulk water has previously been studied in this model using NPT Monte Carlo simulations[28,32−36] and thermodynamic-perturbation and integral equation techniques.[37−40] Those studies have shown that the MB model qualitatively gives many properties of real water, including the density anomaly, the minimum in the isothermal compressibility as a function of temperature, and the thermodynamic properties of nonpolar solvation.[28] Two advantages of the MB model, compared to more realistic water models, are the following: (1) that well-converged computer simulations of thermodynamic properties can be obtained in a reasonable amount of time[28,33−35] and (2) the underlying physical principles can be more readily communicated and visualized in two dimensions.

We have previously used the MB model to study water molecules subject to a different type of constraint, namely, waters within a fixed matrix of Lennard-Jones disks.[40] There, we compared Monte Carlo simulations to the associative replica Ornstein-Zernike equations using the hypernetted chain approximation. We found that the obstacles perturb the network structure of water. Low densities of obstacles lead to increased ordering and hydrogen bonding among the water molecules and increased compressibility, relative to the pure fluid. However, interestingly, high obstacle densities reduce MB water structuring, hydrogen bonding, and compressibility, because the obstacles interfere so extensively with all the possible ways the fluid can form good hydrogen bonding networks.

2. Model

We study MB water that is confined between two planes. Each MB water molecule is a two-dimensional Lennard-Jones disk with three arms separated by an angle of 120° (see Figure 1).[26,28,32,34,35,41] The interaction potential between two MB particles is a sum of a Lennard-Jones term and a hydrogen-bonding (HB) term

$$U(\vec{X}_i,\vec{X}_j) = U_{LJ}(r_{ij}) + U_{HB}(\vec{X}_i,\vec{X}_j) \quad (1)$$

where r_{ij} is the distance between the centers of particles i and j and $\vec{X}_i$ denotes the vector representing the coordinates and the orientation of the ith particle. The Lennard-Jones part of the potential is defined as

$$U_{LJ}(r_{ij}) = 4\epsilon_{LJ}\left(\left(\frac{\sigma_{LJ}}{r_{ij}}\right)^{12} - \left(\frac{\sigma_{LJ}}{r_{ij}}\right)^{6}\right) \quad (2)$$

* Corresponding author.
[†] University of Ljubljana.
[‡] University of California, San Francisco.

10.1021/jp055543f CCC: $33.50
Published on Web 02/16/2006

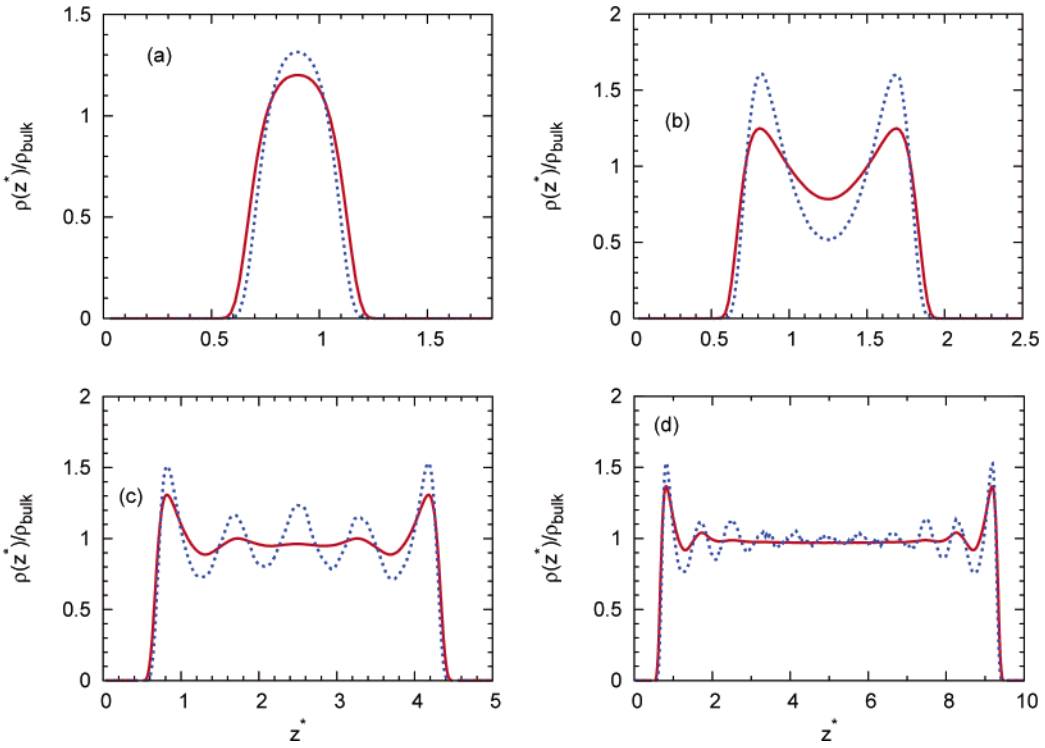

Figure 1. Density profile of MB water between two parallel LJ planes. The blue line presents state point $T^* = 0.18$ and $\rho^* = 0.990$, and the red line presents $T^* = 0.36$ and $\rho^* = 0.534$. The distance between planes is (a) $d = 1.8$, (b) $d = 2.5$, (c) $d = 5.0$, and (d) $d = 10.0$.

where ϵ_{LJ} is the well depth and σ_{LJ} is the contact parameter. The hydrogen-bonding part of the interaction potential is

$$U_{HB}(\vec{X}_i,\vec{X}_j) = \sum_{k,l=1}^{3} U_{HB}^{kl}(r_{ij}, \theta_1, \theta_2) \tag{3}$$

where U_{HB}^{kl} describes the interaction between two arms of different molecules

$$U_{HB}^{kl}(r_{ij}, \theta_1, \theta_2) = \epsilon_{HB} G(r_{ij} - r_{HB})\, G(\vec{l}_k \vec{u}_{ij} - 1)\, G(\vec{j}_l \vec{u}_{ij} + 1) \tag{4}$$

By writing down the scalar products explicitly, we obtain the following form of the HB potential

$$U_{HB}^{kl}(r_{ij}, \theta_i, \theta_j) = \epsilon_{HB} G(r_{ij} - r_{HB})$$
$$G\left(\cos\left(\theta_i + \frac{2\pi}{3}(k-1)\right) - 1\right) G\left(\cos\left(\theta_j + \frac{2\pi}{3}(l-1)\right) + 1\right) \tag{5}$$

where k and l stands for the different arms and $G(x)$ is an unnormalized Gaussian function

$$G(x) = \exp\left(-\frac{x^2}{2\sigma^2}\right) \tag{6}$$

Further, $\epsilon_{HB} = -1$ is an energy parameter and $r_{HB} = 1$ is a characteristic hydrogen bond length. The term $\vec{u}_{ij}$ represents the unit vector along $\vec{r}_{ij}$, and $\vec{l}_k$ is the unit vector representing the kth arm of the ith particle, where θ_i is the orientation of the ith particle. The strongest hydrogen bond occurs when an arm of one particle is collinear with the arm of another particle and the two arms point in opposing directions. The LJ well depth ϵ_{LJ} is 0.1 times the HB interaction energy ϵ_{HB}, and the Lennard-Jones contact parameter σ_{LJ} is $0.7 r_{HB}$.

In the present work, we model the interactions between the MB molecules and the pore walls as

$$\Phi_w(z) = \phi(z) + \phi(d - z) \tag{7}$$

with

$$\phi(z) = 4\epsilon_w\left(\left(\frac{\sigma_w}{z}\right)^9 - \left(\frac{\sigma_w}{z}\right)^3\right) \tag{8}$$

where d is the pore width and $\epsilon_w = \epsilon_{LJ}$ and $\sigma_w = \sigma_{LJ}$ are the parameters of the Lennard-Jones (9, 3) wall-particle potential.

3. Simulation Methods

Computer simulations for MB water between two parallel Lennard-Jones adsorbing surfaces were performed in the (N,V,T) and (μ,V,T) ensembles.

In NVT, we simulated from 100 to 500 MB particles between two walls. At each step, one randomly chosen water molecule is moved. We used periodic boundary conditions and the minimum image convention. The starting configuration of each phase point was selected at random, and the first 1×10^5 moves were discarded as the system equilibrated. Statistics were gathered over the next 1×10^6 moves. In these simulations, the liquid water density in the pore (averaged density) was fixed at the bulk density at a particular temperature. The point of doing these simulations at a constant density is simply to study the water structures at different densities. For the purposes of thermodynamics, we later fix the chemical potential to equal that of the water outside the cavity.

One way to obtain equilibrium with the bulk is to use the grand canonical ensemble.[42] Hence, we also performed μVT simulations. This method has been widely used for the simulation of simple liquids in pores of different types.[43,44] In this approach, the chemical potential of the MB water is specified

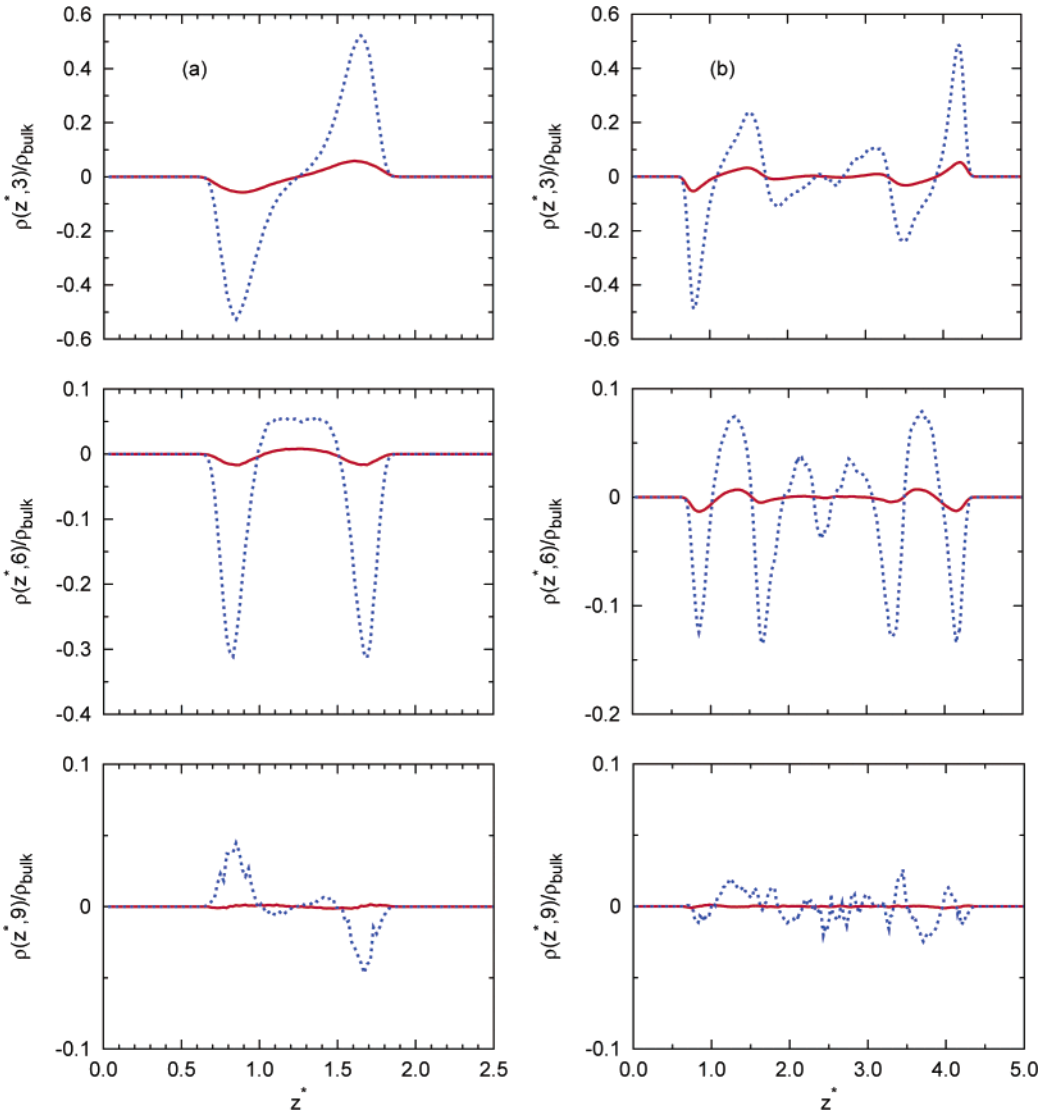

Figure 2. Fourier coefficients of the density profile $\rho(z^*, \theta)$ for water molecules. The first three nonzero harmonics are presented. The blue line presents state point $T^* = 0.18$ and $\rho^* = 0.990$, and the red line presents $T^* = 0.36$ and $\rho^* = 0.534$. The distance between planes is (a) $d = 2.5$ and (b) $d = 5.0$.

and the number of molecules within the pore adjusts itself accordingly. The grand canonical Monte Carlo (GCMC) method has a distinct advantage over constant volume simulations that employ a constant number of molecules in that the appropriate water density is automatically sought in all portions of the system. In μVT, an MB particle is chosen randomly and then moved randomly. The new configuration is accepted in accordance with the classical Metropolis algorithm. When all MB molecules are moved, we try to insert or remove an MB molecule. The starting configuration of each phase point was selected at random, and the first 1×10^5 passes of each particle were discarded as the system equilibrated. Statistics were gathered over the next 1×10^7 moves of each particle. Periodic boundary conditions were used in all simulations to eliminate surface effects.

3.1. Density Profiles and their Fourier Expansion. The profiles of the density, $\rho(z)$, were calculated using standard methods

$$\rho(z) = \frac{\bar{N}}{lh} \tag{9}$$

where $\bar{N}$ is the average number of particles in an interval of width h at distance z from the left plane and l is the dimension of the system parallel to the planes.

The distribution of MB molecules depends on their position z and the angle of the first arm with the normal to the left plane θ. Taking both variables into account, the distribution function is

$$\rho(z, \theta) = \frac{\bar{N}(\theta)}{lh\Delta} \tag{10}$$

where Δ is the interval of orientations. This distribution can be expanded in harmonics

$$\rho(z, \theta) = \sum \rho(z, n) \cos n\theta \tag{11}$$

In simulations, we can calculate this by the following equation[35]

$$\rho(z, n) = \rho(z)\langle \cos n\theta \rangle \tag{12}$$

where $\langle \cos n\theta \rangle$ is the average cosine of an MB particle's orientation multiplied by it's harmonics density component.

4. Results and Discussion

4.1. Density Profiles. Figure 1 shows the computed profiles of water density between planes having different separations.

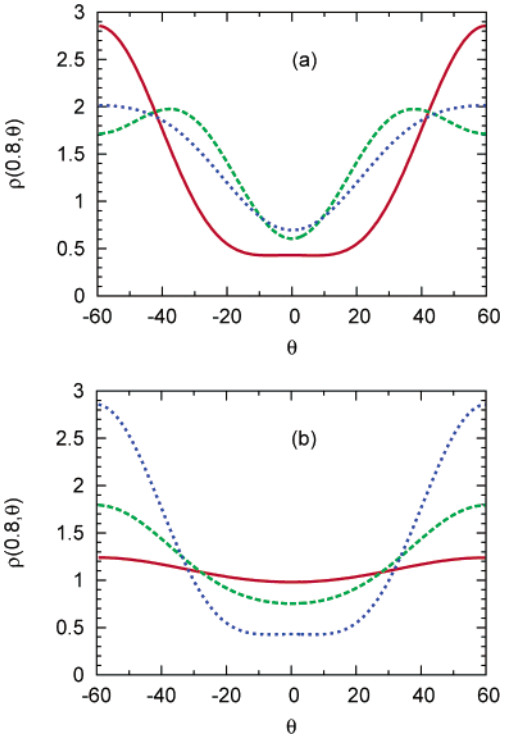

Figure 3. (a) Distance dependence of orientations of MB molecules in contact with the wall. The blue line presents a distance $d = 2.2$, the green line, $d = 2.5$, and the red line, $d = 5.0$. The temperature is equal to $T^* = 0.18$. The parameter θ is the angle between the HB arm and normal vector to the plane. (b) Temperature dependence of orientations of MB molecules in contact with the wall. The blue line presents a temperature $T^* = 0.18$, the green line, $T^* = 0.24$, and the red line, $T^* = 0.36$. The distance between planes is equal to $d = 2.2$.

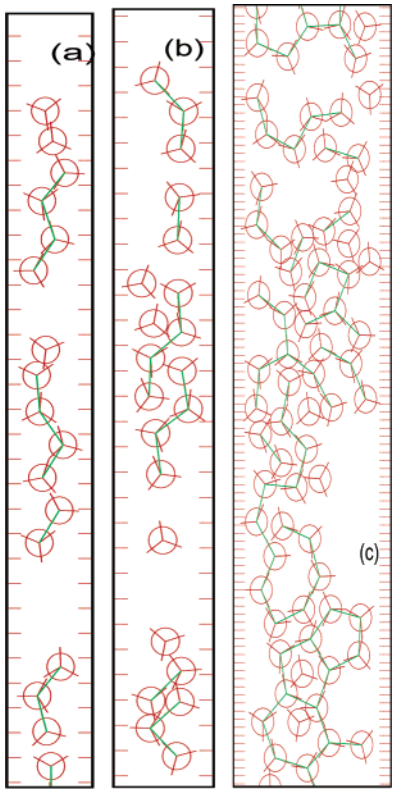

Figure 4. Snapshots of the most dense part of the system for different distances between planes. The distance is equal to (a) $d = 2.2$, (b) $d = 2.5$, and (c) $d = 5.0$. The temperature is $T^* = 0.18$, and the excess chemical potential is $\mu_{ex} = -0.16$. The green lines present hydrogen bonds between MB molecules.

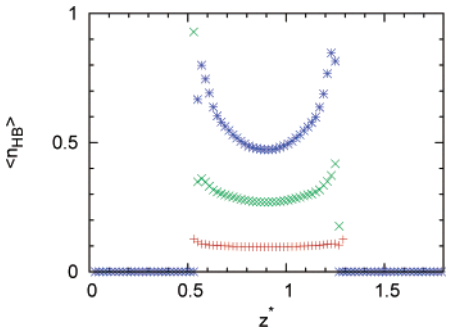

Figure 5. Average number of hydrogen bonds per molecule. Blue symbols present state point $T^* = 0.18$ and $\rho^* = 0.990$, green symbols, $T^* = 0.24$ and $\rho^* = 0.870$, and red symbols, $T^* = 0.36$ and $\rho^* = 0.534$. The distance between planes is $d = 1.8$.

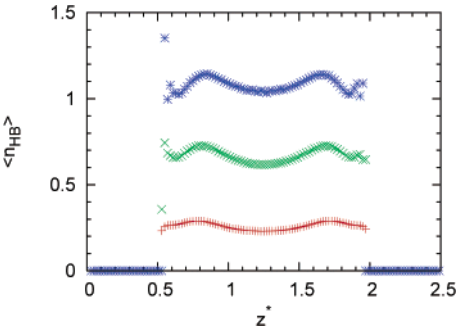

Figure 6. Same plot as Figure 5 with a distance $d = 2.5$.

With small spacings between the planes, $d = 1.8$, there is only room enough for one layer of water. As d increases, allowing more water between the planes, the simulations show that water becomes structured into multiple planar layers between the confining planes. The density of water oscillates along the normal to the planes, due to steric packing and hydrogen bonding. As the temperature is lowered, the structuring increases, the confined-water equivalent of a freezing process. In our reduced units, we refer to $T^* = 0.18$ as cold water and $T^* = 0.36$ as hot water, based on water's behavior in the bulk at those temperatures. Profiles are consistent with the 3D simulations of Choudhury et al.[24,25] for a similar type of potential.

4.2. Fourier Expansion of Density Profiles. Figure 2a and b shows the Fourier expansion of the density profiles for $d = 2.5$ and $d = 5.0$, respectively. A key conclusion from this figure is that it is sufficient to retain only the first three Fourier components to accurately capture the density variations. The implication is that analytical modeling might be done efficiently using a density functional theory with only a few dominant terms.

4.3. Angular Distributions. Figure 3a plots the orientations of the cold water molecules ($T^* = 0.18$) that are in contact with the wall, for different cavity sizes. The angle zero represents an arm pointing away from the left plane, normal to the plane. It shows that, in the smallest and largest cavities, water molecules have a preference to "waste" a hydrogen bond by pointing it directly at the wall. Figure 3b also shows waters at the walls, but now for a single cavity, $d = 2.2$, as a function of temperature. It shows the increased orientational structuring of the water as the temperature is lowered.

Orientation dependence of the size of the pore can be understood in terms of the graphic in Figure 4, showing the properties of confined water under three different conditions. First, when there is a small distance between planes, the water forms zigzag chains along the pore. At a distance $d = 2.5$, the chains are

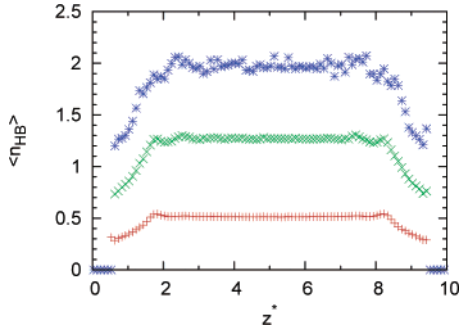

Figure 7. Same plot as Figure 5 with a distance $d = 10.0$.

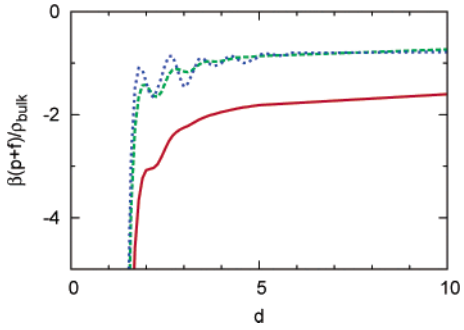

Figure 8. Distance dependence of the force between planes. The blue line presents a temperature $T^* = 0.18$, the green line, $T^* = 0.24$, and the red line, $T^* = 0.40$. The excess chemical potential is a constant equal to $\mu_{ex} = -0.16$.

slightly different and this affects the orientation of water molecules in contact with the wall. When the distance between the walls is higher, the waters point one arm toward the wall.

4.4. Hydrogen-Bonding Networks. Figures 5 ($d = 1.8$), 6 ($d = 2.5$), and 7 ($d = 10.0$) show the distributions in the average number of hydrogen bonds of each water molecule, as a function of temperature and plane separation, d. In small cavities, water is not able to satisfy many of its potential hydrogen bonds. The thermal properties of water do not begin to show bulklike distributions until the planes are separated by around 10 water diameters. This hydrogen-bonding property is consistent with others above in showing that lowering the temperature leads to more water ordering, for a given cavity size.

4.5. Thermodynamic Properties. *4.5.1. Forces between Plates.* Intervening water will exert a force on its two confining plates. The external force required to hold the two plates in equilibrium can depend on the plate separation, d. Figure 8 shows how this applied equilibrium pressure depends on the plate separation, in our MB model simulations, calculated using (see, for example, ref 46):

$$f\beta + p\beta = \int \frac{\partial \Phi_w(z)}{\partial z} \rho(z)\, dz \qquad (13)$$

where f is the force applied to push the planes together, p is the pressure of the bulk MB water, and $\rho(z)$ is the water density profile.

Mica-plate force experiments of this type have been performed by Israelachvili and others.[45] It was shown that there are large oscillations in the profile of force vs plate separation, d, and that the oscillations persist even when the planes are separated by up to 10 water diameters. The present simulations are consistent with these two observations and indicate that the walls can affect water structuring even 5−20 water diameters away.

We find that increased temperature should decrease the amplitude of these oscillations. As far as we know, there is no experiment yet of this type.

4.5.2. Excess Energy, Heat Capacity, and Isothermal Compressibility. An advantage of using our simple MB model is that we can obtain computational convergence for fluctuation

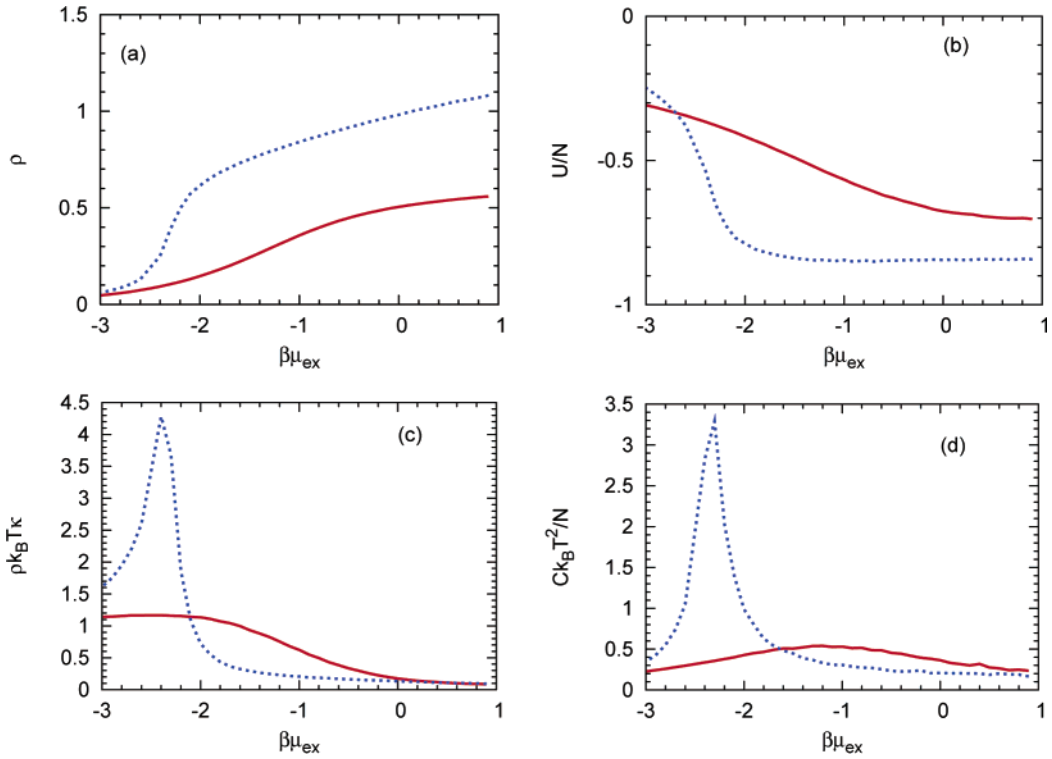

Figure 9. Density (a), internal energy (b), isothermal compressibility (c), and heat capacity (d) of MB molecules between two parallel planes vs excess chemical potential of MB molecules for different distances between planes. The red line presents a distance $d = 2.0$, and the blue line presents $d = 5.0$. Temperature in both cases is equal to $T^* = 0.18$.

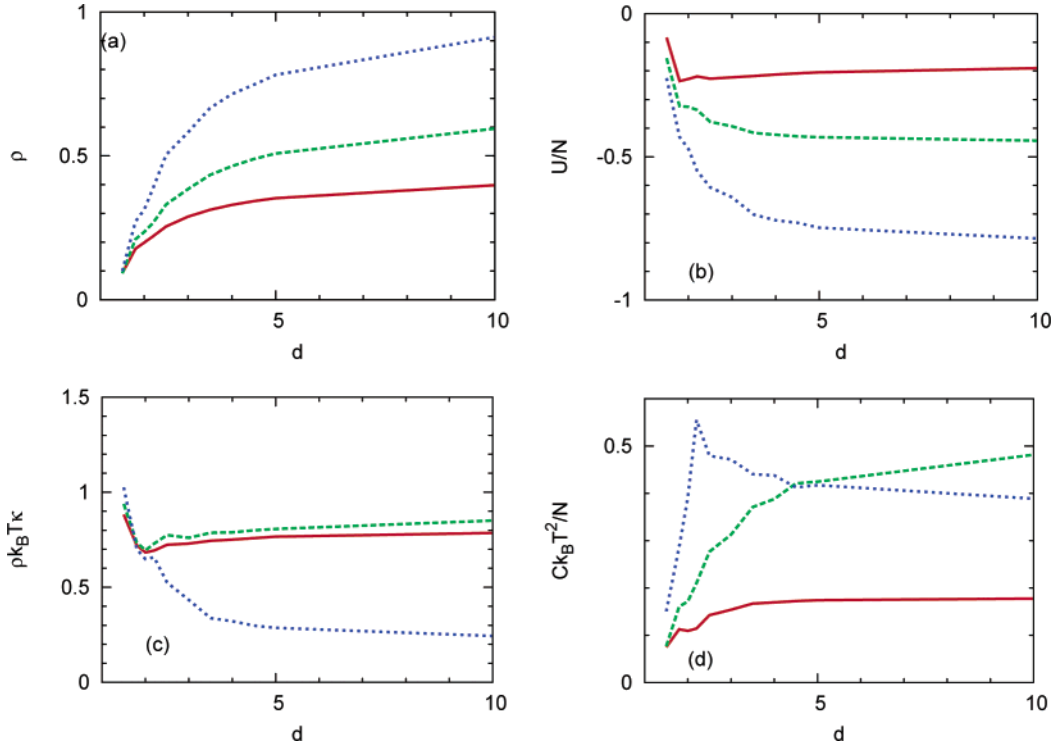

Figure 10. Density (a), internal energy (b), isothermal compressibility (c), and heat capacity (d) of MB molecules between two parallel planes vs the distance between planes. The blue line present temperature $T^* = 0.20$, the green line, $T^* = 0.26$, and the red line, $T^* = 0.40$. The excess chemical potential is a constant equal to $\mu_{ex} = -0.16$.

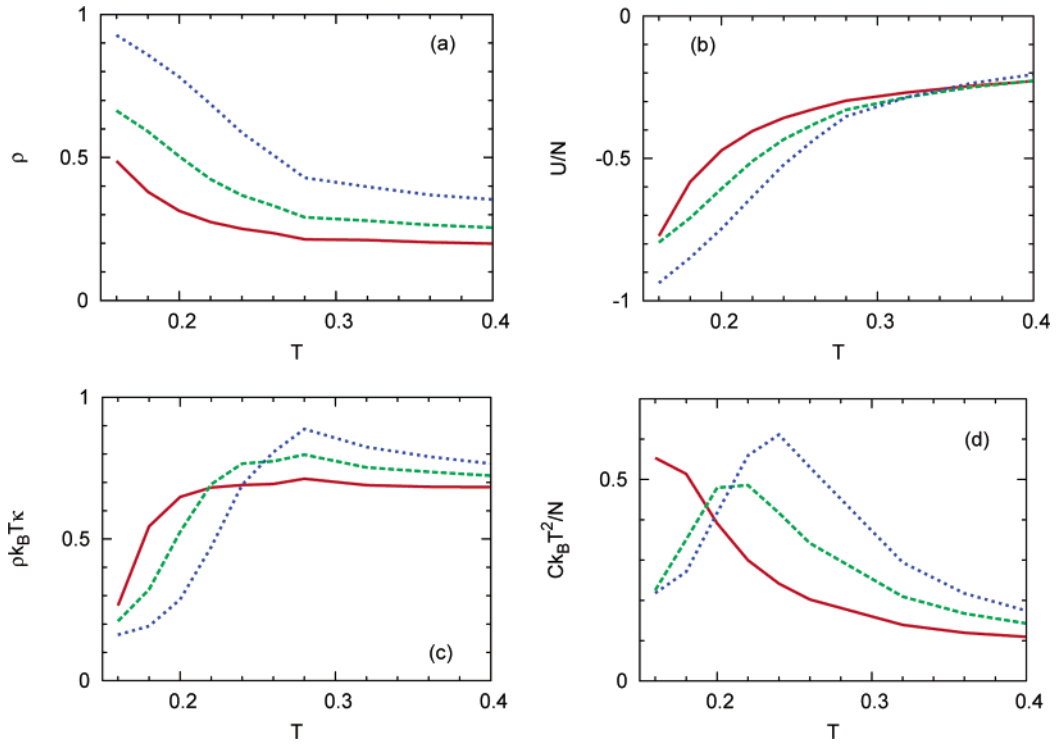

Figure 11. Density (a), internal energy (b), isothermal compressibility (c), and heat capacity (d) of MB molecules between two parallel planes vs temperature for different distances between planes at a constant chemical potential $\mu_{ex} = -0.16$. The red line presents a distance $d = 2.0$, the green line, $d = 2.5$, and the blue line, $d = 5.0$.

properties, such as the heat capacity and compressibility, which are computationally much more costly for all-atom three-dimensional model simulations. The heat capacity is an important fingerprint of water's thermal properties.

The natural choice of an ensemble in adsorption studies is the Grand canonical ensemble. The fluid in a nanopore is in equilibrium with the bulk liquid at the same chemical potential. A sufficiently large positive chemical potential of water in the bulk will cause water to escape from the bulk to fill the pore.

Figure 9 shows various thermal properties of cold confined water (density ρ, energy U_p, heat capacity C, and isothermal compressibility κ) as a function of the excess chemical potential

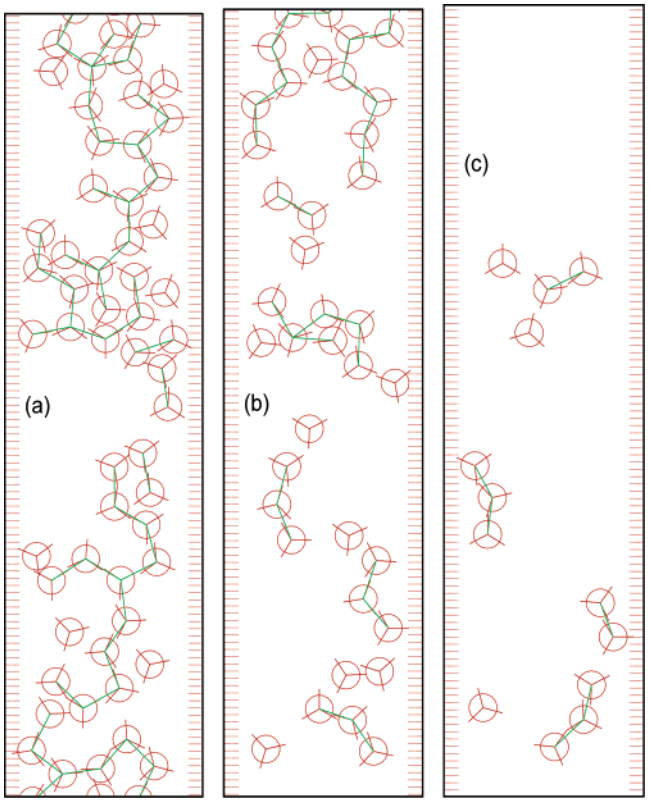

Figure 12. Snapshots of the most dense part of the system for different excess chemical potentials of MB molecules. The excess chemical potential is equal to (a) $\beta\mu_{ex} = -2.0$, (b) $\beta\mu_{ex} = -2.3$, and (c) $\beta\mu_{ex} = -2.8$. The temperature is $T^* = 0.18$, and distance is $d = 5.0$. Green lines present hydrogen bonds between MB molecules. We say that a hydrogen bond is formed when the HB interaction is stronger than the LJ interaction.

μ_{ex}, for a small cavity ($d = 2$, red line) and a larger cavity ($d = 5$, blue line).

One way to interpret the heat capacity is as a mode of storage of energy as the temperature is increased. In typical hydrophobicity problems, this mode of energy storage (energy increase) is the breaking of hydrogen bonds with increasing temperature. Here, we see an interesting effect. The heat capacity is largest for a pore size of 2.2. For smaller cavities, water molecules cannot form spatially extended hydrogen-bonding networks. In particular, in small pores, waters are largely isolated or occur in single pairs of hydrogen-bonded molecules. For cavities larger than 2.2, extensive hydrogen-bonding networks can form. At an exact pore size of 2.2, water approximately forms a long one-dimensional chain, hence allowing for energy storage in the chain structure. This is the reason that the heat capacity is maximal for a pore size that is just about two water molecules in width.

The thermal properties (Figures 9, 10, and 11) can be understood in terms of the graphic in Figure 12, showing the properties of confined water under three different conditions. First, when there is little water in the pore, the water is in a gaslike low-density state. Its compressibility is high, as it would be for gas-phase water in the bulk. There are few hydrogen bonds. Second, when there is much water in the pore, it is in a higher density liquidlike state. It's compressibility is lower. Water forms highly connected hydrogen-bonded networks, as in liquid water.

Third, there will be a state that is intermediate between these two, where a transition occurs, depending on the temperature, cavity size d, and external water chemical potential, $\beta\mu_{ex}$. This is the transition from a low density to a high density of water in the pore. For example, for $d = 5.0$, the thermodynamic properties show a transition at $\beta\mu_{ex} = -2.3$. This state is indicated in Figure 12b. In this intermediate state, the system is poised to go either way; it easy to make or break new hydrogen bonds. A system that can readily break hydrogen bonds with only a small increase in temperature has a high heat capacity, hence our observed heat capacity peaks. The fluctuations in density and hydrogen bonding are larger in this state than in the low-density or high-density states. It resembles a sort of boiling point, which depends not only on the temperature but also on the pore properties, μ_{ex} and d.

There is pronounced density variation along the pore in the later case. Within the pore, there are large density variations in some places that water is clustered; in other places, there are significant holes, without water molecules.

The computer simulations of Brovchenko et al.[17] performed for TIP4P water in hydrophobic nanopores support this picture. Both the heat capacity and isothermal compressibility variations with μ_{ex} reflect the situation illustrated by snapshots of water distributions taken at four different values of the excess chemical potential. At very high chemical potential, however, the MB water molecules form the connected network through the entire pore; the behavior of the fluid is now more similar to that of the bulk system (Figure 12c).

These predictions from the MB model are supported by recent calorimetry experiments of Tombari et al.[47] on water and ice confined within Vycor glass 2 nm nanopores. They show that (i) at low temperatures the heat capacity of water increases on nanoconfinement, (ii) the measured heat capacity is a nonmonotonic function of temperature (cf. Figure 3a of ref 47), leading to an asymmetric maximum similar to those shown in our Figure 9d, (iii) C increases more at low filling of the pores (lower excess chemical in our case), (iv) the C decreases with increasing amounts of confined water. A more detailed comparison between our model calculations and the experimental work is difficult since Vycor nanopores are partly hydrophilic (see ref 17).

5. Conclusions

We use the simple two-dimensional MB model of water to study the properties of water confined within pores and cavities. Bulk water will boil when heated. In pores, the boiling point of water also depends on the pore size and the excess chemical potential of the water. We find that waters confined between two planes will be structured by the planes so that the density and hydrogen bonding oscillates across the channel and structuring occurs even when channels are 10 times the size of a water molecule.

While our model does not accurately capture the 3D geometry of water, the main value of it is in exploring the tradeoff between spherically symmetrical Lennard−Jones interactions of spherical particles in confined spaces with orientation-dependent hydrogen bonding. We find that confinement clearly alters the orientational distributions of particles because hydrogen bonding is involved.

Acknowledgment. This work was supported by the Slovenian Research Agency (Physical Chemistry Research Program 0103-0201 and Research Project J1-6653) and NIH Grant GM063592. T.U. gratefully acknowledges a Fulbright fellowship from the Bureau of Educational and Cultural Affairs of the U.S. Department of State.

References and Notes

(1) Hummer, G.; Rasaiah, J. C.; Noworyta, J. P. *Nature* **2001**, *414*, 188.

(2) de Groot, B. L,; Grubmüller, H. *Curr. Opin. Struct. Biol.* **2005**, *15*, 176.
(3) Vidossich, P.; Cascella, M.; Carloni, P. *Proteins* **2004**, *55*, 924.
(4) Bellisent-Funnel, M. C.; Sridi-Dorbez, R.; Bosio, L. *J. Chem. Phys.* **1996**, *104*, 10023.
(5) Bratko, D.; Luzar, A.; Blum, L. *J. Chem. Phys.* **1987**, *86*, 2955.
(6) Bruni, F.; Ricci, M. A.; Soper, A. K. *J. Chem. Phys.* **1998**, *109*, 1478.
(7) Soper, A. K.; Bruni, F.; Ricci, M. A. *J. Chem. Phys.* **1998**, *109*, 1486.
(8) Dore, J. C. *Chem. Phys.* **2000**, *258*, 327.
(9) Scodinu, A.; Fourkas, J. T. *J. Phys. Chem. B* **2002**, *106*, 10292.
(10) Crupi, V.; Majolino, D.; Migliardo, P.; Venutti, V. *J. Phys. Chem. B* **2002**, *106*, 10884.
(11) Hartnig, C.; Witschel, W.; Spohr, E.; Gallo, P.; Ricci, M. A.; Rovere, M. *J. Mol. Liq.* **2000**, *85*, 127.
(12) Bratko, D.; Curtis, R. A.; Blanch, H. W.; Prausnitz, J. M. *J. Chem. Phys.* **2001**, *115*, 3873.
(13) Giaya, A.; Thompson, R. W. *J. Chem. Phys.* **2002**, *116*, 2565.
(14) Brovchenko, I.; Geiger, A. *J. Mol. Liq.* **2002**, *96*, 195.
(15) Berezhkovskii, A.; Hummer, G. *Phys. Rev. Lett.* **2002**, *89*, 064503.
(16) Waghe, A.; Rasaiah, J. C.; Hummer, G. *J. Chem. Phys.* **2002**, *117*, 10789.
(17) Brovchenko, I.; Geiger, A.; Oleinikova, A.; Paschek, D. *Eur. Phys. J. E* **2003**, *12*, 69.
(18) Maibaum, L.; Chandler, D. *J. Phys. Chem. B* **2003**, *107*, 1189.
(19) Scatena, L. F.; Brown, M. G.; Richmond, G. L. *Science* **2001**, *292*, 908.
(20) Webber, B.; Dore, J. *J. Phys.: Condens. Matter* **2004**, *16*, S5449.
(21) Vaitheeswaran, S.; Rasaiah, J. C.; Hummer, G. *J. Chem. Phys.* **2004**, *121*, 7955.
(22) Floquet, N.; Coulomb, J. P.; Dufau, N.; Andre, G.; Kahn, R. *Physica B* **2004**, *350*, 265.
(23) Zangi, R. *J. Phys.: Condens. Matter* **2004**, *16*, S5371.
(24) Choudhury, N.; Pettitt, B. M. *J. Am. Chem. Soc.* **2005**, *127*, 3556.
(25) Choudhury, N.; Pettitt, B. M. *Mol. Simul.* **2005**, *31*, 457.
(26) Ben-Naim, A. *J. Chem. Phys.* **1971**, *54*, 3682.
(27) Ben-Naim, A. *Mol. Phys.* **1972**, *24*, 705.
(28) Silverstein, K. A. T.; Haymet, A. D. J.; Dill, K. A. *J. Am. Chem. Soc.* **1998**, *120*, 3166.
(29) Silverstein, K. A. T.; Haymet, A. D. J.; Dill, K. A. *J. Chem. Phys.* **1999**, *111*, 8000.
(30) Silverstein, K. A. T.; Haymet, A. D. J.; Dill, K. A. *J. Am. Chem. Soc.* **2000**, *122*, 8037.
(31) Dill, K. A.; Truskett, T. M.; Vlachy, V.; Hribar-Lee, B. *Annu. Rev. Biophys. Biomol. Struct.* **2005**, *34*, 173.
(32) Andaloro, G.; Sperandeo-Mineo, R. M. *Eur. J. Phys.* **1990**, *11*, 275.
(33) Haymet, A. D. J.; Silverstein, K. A. T.; Dill, K. A. *Faraday Discuss.* **1996**, *103*, 117.
(34) Southall, N. T.; Dill, K. A. *J. Phys. Chem. B* **2000**, *104*, 1326.
(35) Silverstein, K. A. T.; Dill, K. A.; Haymet, A. D. J. *J. Chem. Phys.* **2001**, *114*, 6303.
(36) Hribar, B.; Southall, N. T.; Vlachy, V.; Dill, K. A. *J. Am. Chem. Soc.* **2002**, *124*, 12302.
(37) Urbic, T.; Vlachy, V.; Kalyuzhnyi, Yu. V.; Southall, N. T.; Dill, K. A. *J. Chem. Phys.* **2000**, *112*, 2843.
(38) Urbic, T.; Vlachy, V.; Kalyuzhnyi, Yu. V.; Southall, N. T.; Dill, K. A. *J. Chem. Phys.* **2002**, *116*, 723.
(39) Urbic, T.; Vlachy, V.; Kalyuzhnyi, Yu. V.; Dill, K. A. J. *J. Chem. Phys.* **2003**, *118*, 5516.
(40) Urbic, T.; Vlachy, V.; Pizio, O.; Dill, K. A. *J. Mol. Liq.* **2004**, *112*, 71.
(41) Silverstein, K. A. T.; Dill, K. A.; Haymet, A. D. J. *Fluid Phase Equilib.* **1998**, *120*, 3166.
(42) Valleau, J. P.; Cohen, L. K. *J. Chem. Phys.* **1980**, *72*, 5935.
(43) Shelly, L. D.; Pattey, G. N.; Berard, D. R.; Torrie, G. M. *J. Chem. Phys.* **1997**, *107*, 2122.
(44) Delville, A. *J. Phys. Chem.* **1993**, *97*, 9703.
(45) Israelachvili, J.; Pashley, R. M. *Nature* **1983**, *306*, 249.
(46) Huerta, A.; Sokolowski, S.; Pizio, O. *Mol. Phys.* **1999**, *97*, 919.
(47) Tombari, E.; Salvetti, G.; Ferrari, C.; Johari, G. P. *J. Chem. Phys.* **2005**, *122*, 104712.